

Surface Enzyme Kinetics for Biopolymer Microarrays: a Combination of Langmuir and Michaelis–Menten Concepts

Hye Jin Lee, Alastair W. Wark, Terry T. Goodrich, Shiping Fang, and Robert M. Corn*

Department of Chemistry, University of California-Irvine, Irvine, California 92697

Received December 21, 2004. In Final Form: February 14, 2005

Real-time surface plasmon resonance (SPR) imaging measurements of surface enzymatic reactions on DNA microarrays are analyzed using a kinetics model that couples the contributions of both enzyme adsorption and surface enzyme reaction kinetics. For the case of a 1:1 binding of an enzyme molecule (E) to a surface-immobilized substrate (S), the overall enzymatic reaction can be described in terms of classical Langmuir adsorption and Michaelis–Menten concepts and three rate constants: enzyme adsorption (k_a), enzyme desorption (k_d) and enzyme catalysis (k_{cat}). In contrast to solution enzyme kinetics, the amount of enzyme in solution is in excess as compared to the amount of substrate on the surface. Moreover, the surface concentration of the intermediary enzyme–substrate complex (ES) is not constant with time, but goes to zero as the reaction is completed. However, kinetic simulations show that the fractional surface coverage of ES on the remaining unreacted sites does reach a steady-state value throughout the course of the surface reaction. This steady-state value approaches the Langmuir equilibrium value for cases where $k_a[E] \gg k_{cat}$. Experiments using the 3' → 5' exodeoxyribonuclease activity of Exonuclease III on double-stranded DNA microarrays as a function of temperature and enzyme concentration are used to demonstrate how this model can be applied to quantitatively analyze the SPR imaging data.

I. Introduction

The parallel enzymatic processing of biopolymer microarrays is rapidly becoming an integral component in the creation of many novel surface-based biotechnologies and bioaffinity sensor applications. Enzymes are attractive tools for surface bioengineering for a number of reasons: surface enzyme reactions are highly specific and result in selective surface site modifications, work under biocompatible conditions often with high efficiency, and in some cases, are reversible. For example, we have recently demonstrated the use of RNase H to enzymatically amplify the signal in surface plasmon resonance (SPR) imaging measurements on nucleic acid microarrays and have also used SPR imaging to monitor the cleavage of peptide arrays with the enzyme Factor Xa.^{1,2} Other researchers have used single-base-extension enzyme reactions on DNA microarrays to detect single nucleotide polymorphisms (SNPs).³ In addition to biosensing applications, the implementation of DNA computing algorithms on surfaces also requires the processing of immobilized oligonucleotides with various DNA enzymes.⁴ Directed enzymatic cleavage of an oligonucleotide monolayer has also been applied to create nanometer-scale surface patterns.^{5,6}

A simple reaction scheme for the enzymatic processing of surface biopolymers is shown in Figure 1. The enzyme (E) first adsorbs from solution onto the surface-bound

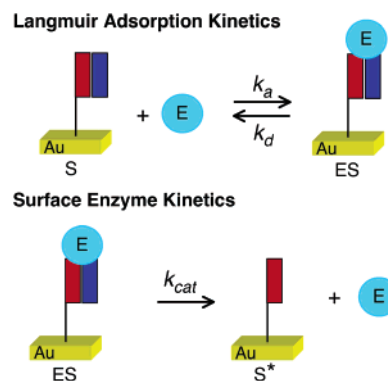


Figure 1. A reaction scheme showing the surface enzymatic processing of a biopolymer microarray.

substrate (S) to create the surface complex (ES). The surface complex then reacts to form the surface-bound product (S^*). This reaction scheme differs from the typical enzymatic method for detecting species on surfaces, which uses a sandwich assay in which an enzyme–protein conjugate binds to an adsorbed molecule and then reacts with a substrate in solution to create an amplified detection signal (optical, electrochemical, etc.).^{7,8} In contrast, the substrate in the enzyme reaction scheme presented in Figure 1 is surface-bound and therefore limited in number as compared to the enzyme in solution. Moreover, the reaction of the surface enzyme complex releases the enzyme back into solution.

Despite the attractive features of enzymes as surface biochemical tools, there are to date very few researchers that have quantitatively considered the kinetics and thermodynamics of enzyme-catalyzed surface reactions.

* Author to whom correspondence should be addressed. E-mail: rcorn@uci.edu.

(1) Goodrich, T. T.; Lee, H. J.; Corn, R. M. *Anal. Chem.* **2004**, *76*, 6173–6178.

(2) Wegner, G. J.; Wark, A. W.; Lee, H. J.; Codner, E.; Saeki, T.; Fang, S.; Corn, R. M. *Anal. Chem.* **2004**, *76*, 5677–5684.

(3) Giusto, D. D.; King, G. C. *Nucl. Acids Res.* **2003**, *31*, e7.

(4) Frutos, A. G.; Condon, A. E.; Smith, L. M.; Corn, R. M. *J. Am. Chem. Soc.* **1998**, *120*, 10277–10282.

(5) Jang, C.; Stevens, B. D.; Carrier, P. R.; Calter, M. A.; Ducker, W. A. *J. Am. Chem. Soc.* **2002**, *124*, 12114–12115.

(6) Hyun, J.; Kim, J.; Craig, S. L.; Chilkoti, A. *J. Am. Chem. Soc.* **2004**, *126*, 4770–4771.

(7) Crowther, J. R. *ELISA: Theory and Practice*, 1st ed.; Humana Press Inc.: Totowa, NJ, 1995; Vol. 42.

(8) Bourdillon, C.; Demaille, C.; Moiroux, J.; Saveant, J. J. *J. Am. Chem. Soc.* **1999**, *121*, 2401–2408.

In a series of papers, Gast et al. have examined the reaction of collagenase on peptide monolayers^{9–11} and the reaction of protease on BSA monolayers.¹² For the case of protease adsorption and reaction, they proposed a modified Michaelis–Menten model for the surface kinetics. However, the authors restricted their kinetic analysis to the later stage of the reaction with over 75% of the substrate removed.¹² For this time regime, the adsorption kinetics and surface enzyme reaction are decoupled.

To study surface enzymatic reaction rates quantitatively, various analytical approaches have been employed to directly monitor the surface process in real-time and discriminate against possible bulk signal contribution. While most research efforts have focused on the use of fluorescence-based detection methods,^{9,10,13–16} SPR-based techniques have recently gained more attention due to the distinct advantage of being “label-free” such that the inconvenience and potential alteration of biological activity associated with fluorescent tags is avoided.^{1,2,17–22} For example, Robertson et al.¹² have employed a combination of SPR and surface plasmon enhanced fluorescence to create separate profiles of the enzyme adsorption and substrate cleavage steps. In addition, we have demonstrated that time-resolved SPR imaging measurements can be used to study Langmuir adsorption kinetics and enzyme reaction kinetics on surfaces.²

In this paper, we propose a novel approach to the quantitative analysis of enzyme-catalyzed surface reactions that couples both adsorption kinetics and enzyme kinetics to quantitatively describe the reaction of an enzyme in solution with a surface-immobilized substrate. We find that the surface coverage of the enzyme–substrate intermediate is governed by an interesting combination of classical Langmuir adsorption kinetics and Michaelis–Menten concepts. As an example, we investigate the exodeoxyribonuclease activity of Exonuclease III on well-characterized double-stranded DNA (dsDNA) microarrays.^{23,24} The kinetics of the selective 3′ → 5′ Exo III hydrolysis of one strand of the two DNA strands in a DNA duplex was monitored at various temperatures using the multiplexed technique of real-time SPR imaging.^{1,2} For the Exo III surface reaction at 20 °C, the SPR signal initially increased due to enzyme adsorption and then

decreased as the surface exonuclease reaction went to completion. This real-time SPR response was monitored at various bulk enzyme concentrations and analyzed using the proposed surface kinetic model to achieve further insight into the relative contributions of the enzyme adsorption and catalytic steps to the overall reaction rate.

II. Theoretical Considerations

Figure 1 depicts a reaction scheme for the surface enzymatic processing of a biopolymer microarray where the enzyme binds specifically to an immobilized substrate molecule in a simple 1:1 ratio. In the absence of bulk transport limitations, the reaction steps can be represented in the form:



where S is the surface bound substrate, E is the enzyme in solution, ES is the surface bound enzyme–substrate complex, and S^* is the surface bound product. Assuming that enzyme adsorption and desorption are described by simple Langmuir kinetics, the reaction rates for the production of ES and S^* can be given by eqs 3 and 4:

$$\frac{d\Gamma_{ES}}{dt} = k_a\Gamma_S[E] - k_d\Gamma_{ES} - k_{\text{cat}}\Gamma_{ES} \quad (3)$$

$$\frac{d\Gamma_{S^*}}{dt} = k_{\text{cat}}\Gamma_{ES} \quad (4)$$

where Γ denotes a surface coverage. If Γ_{tot} is the total number of surface sites, then the reaction rates can be expressed in terms of the relative surface coverages, $\theta_x = \Gamma_x/\Gamma_{\text{tot}}$, where $x = S, ES$ or S^* :

$$\theta_S + \theta_{ES} + \theta_{S^*} = 1 \quad (5)$$

$$\frac{d\theta_{ES}}{dt} = k_a\theta_S[E] - k_d\theta_{ES} - k_{\text{cat}}\theta_{ES} \quad (6)$$

$$\frac{d\theta_{S^*}}{dt} = k_{\text{cat}}\theta_{ES} \quad (7)$$

The solution of the coupled surface kinetics eqs 6 and 7 depends on the relative values of the rate constants k_a, k_d , and k_{cat} .

A. Steady-State Solution for Slow Surface Enzyme Kinetics. If the surface enzyme reaction is very slow as compared to the adsorption process ($k_{\text{cat}} \ll k_a, k_d$), then we can assume that surface coverage of the intermediate ES is constant ($d\theta_{ES}/dt = 0$) and we can solve eq 6 for θ_{ES} :

$$\theta_{ES} = \frac{k_a\theta_S[E]}{k_d + k_{\text{cat}}} = \frac{\theta_S[E]}{K'_M} \quad (8)$$

where K'_M is defined as the “surface” Michaelis–Menten constant:

$$K'_M = \frac{k_d + k_{\text{cat}}}{k_a} \quad (9)$$

(9) Gaspers, P. B.; Robertson, C. R.; Gast, A. P. *Langmuir* **1994**, *10*, 2699–2704.

(10) Gaspers, P. B.; Gast, A. P.; Robertson, C. R. *J. Colloid Interface Sci.* **1995**, *172*, 518–529.

(11) Trigianto, G.; Gast, A. P.; Robertson, C. R. *J. Colloid Interface Sci.* **1999**, *213*, 81–86.

(12) Kim, J.; Roy, S.; Kellis, J. T., Jr.; Poulou, A. J.; Gast, A. P.; Robertson, C. R. *Langmuir* **2002**, *18*, 6312–6318.

(13) Jervis, E. J.; Haynes, C. A.; Kilburn, D. G. *J. Biol. Chem.* **1997**, *272*, 24016–24023.

(14) Tachi-iri, Y.; Ishikawa, M.; Hirano, K. *Anal. Chem.* **2000**, *72*, 1649–1656.

(15) Bosma, A. Y.; Ulijn, R. V.; McConnell, G.; Girkin, J.; Halling, P. J.; Flitsch, S. L. *Chem. Commun.* **2003**, *22*, 2790–2791.

(16) Tawa, K.; Knoll, W. *Nucl. Acids Res.* **2004**, *32*, 2372–2377.

(17) Peterson, A. W.; Wolf, L. K.; Georgiadis, R. M. *J. Am. Chem. Soc.* **2002**, *124*, 14601–14607.

(18) Goodrich, T. T.; Lee, H. J.; Corn, R. M. *J. Am. Chem. Soc.* **2004**, *126*, 4086–4087.

(19) Shumaker-Parry, J. S.; Campbell, C. T. *Anal. Chem.* **2004**, *76*, 907–917.

(20) Shumaker-Parry, J. S.; Zareie, M. H.; Aebersold, R.; Campbell, C. T. *Anal. Chem.* **2004**, *76*, 918–929.

(21) Kyo, M.; Yamamoto, T.; Motohashi, H.; Kamiya, T.; Kuroita, T.; Tanaka, T.; Engel, J. D.; Kawakami, B.; Yamamoto, M. *Genes Cells* **2004**, *9*, 153–164.

(22) Kanda, V.; Kariuki, J. K.; Harrison, D. J.; McDermott, M. T. *Anal. Chem.* **2004**, *76*, 7257–7262.

(23) Nelson, B. P.; Grimsrud, T. E.; Liles, M. R.; Goodman, R. M.; Corn, R. M. *Anal. Chem.* **2001**, *73*, 1–7.

(24) Lee, H. J.; Goodrich, T. T.; Corn, R. M. *Anal. Chem.* **2001**, *73*, 5525–5531.

This definition is analogous to the definition of the normal solution Michaelis–Menten constant.²⁵ Initially, the amount of product, S^* , on the surface is small and can be neglected in eq 5. We define θ'_{ES} as the steady-state surface coverage of the intermediate ES for this case. Using eq 5 to replace θ_S in eq 8 with $1 - \theta'_{ES}$ leads to the following equation:

$$\theta'_{ES} = \frac{[E]}{K'_M + [E]} \quad (10)$$

Equation 10 has the same functional form as that observed in solution Michaelis–Menten enzyme kinetics, $[ES]/E_{\text{tot}} = [S]/(K_M + [S])$,²⁵ but the surface reaction rate is a function of solution enzyme concentration ($[E]$) instead of surface substrate concentration ($[S]$). This is because, in the solution reaction, the substrate is typically in excess relative to the enzyme, whereas for surface enzyme kinetics, the enzyme in solution is in excess relative to the substrate on the surface.

Equation 10 can also be described as a “dynamic” Langmuir adsorption isotherm for the surface enzyme complex. If k_{cat} is much smaller than k_d , then the surface Michaelis–Menten constant, K'_M , in eq 9 becomes the inverse of the Langmuir adsorption coefficient, $K_{\text{Ads}} = k_d/k_{\text{cat}}$, and eq 10 becomes the normal equilibrium Langmuir adsorption isotherm and the surface coverage reaches its equilibrium value (θ_{ES}^{eq}):

$$\theta_{ES}^{\text{eq}} = \frac{K_{\text{Ads}}[E]}{1 + K_{\text{Ads}}[E]} \text{ if } k_{\text{cat}} \ll k_d \quad (11)$$

Thus, we find that the initial rate of the surface enzyme reaction is proportional to the steady-state coverage of the intermediate ES , and the inverse of the surface Michaelis–Menten constant can be thought of as a “dynamic” Langmuir adsorption coefficient that controls the ES surface coverage. If the reaction is very slow, then this steady-state surface coverage is the same as the equilibrium ES surface coverage as given by the Langmuir adsorption isotherm.

B. General Solution and Surface Simulations. If k_{cat} is equal to or greater than $k_a[E]$, then we cannot make the steady-state assumption that the surface ES concentration is constant and the surface S^* concentration is negligible. Instead, kinetic simulations of eqs 6 and 7 must be used to follow the temporal evolution of the relative surface coverages during the course of the enzymatic reaction.

The kinetic simulations are easily performed using Euler integration methods with the initial conditions that $\theta_S = 1$, $\theta_{ES} = 0$, and $\theta_{S^*} = 0$ at time $t = 0$ (we actually reduce the problem to only two variables by eliminating θ_S from eq 6 by using eq 5). An example of a kinetic simulation is shown in Figure 2 where k_{cat} and $k_a[E]$ are arbitrarily set equal to 0.25 s^{-1} and k_d is set to 0.025 s^{-1} . As seen in this figure, the surface coverage of S (θ_S) drops monotonically to zero as the relative surface coverage of the product S^* (θ_{S^*}) monotonically increases to one as the reaction is completed. The relative surface coverage of the intermediate ES (θ_{ES}) is not constant during the course of the reaction but instead rises to a maximum value of 0.38 after $\sim 4 \text{ s}$, and then slowly decreases to zero. It never

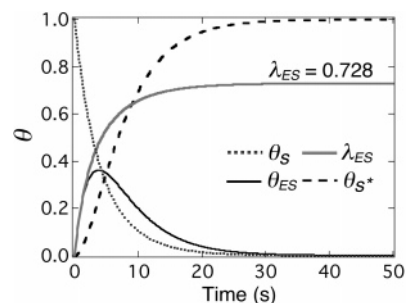


Figure 2. Kinetic simulation of the surface enzyme reactions defined in eqs 5–7. For this simulation, $k_a[E] = k_{\text{cat}} = 0.25 \text{ s}^{-1}$; $k_d = 0.025 \text{ s}^{-1}$. The steady-state value for λ_{ES} is 0.728.

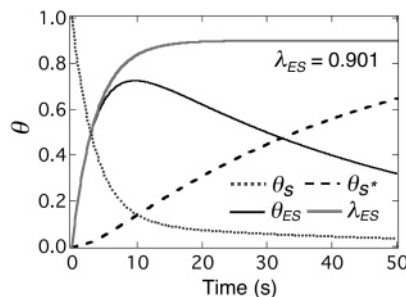


Figure 3. Kinetic simulation of the surface enzyme reactions defined in eqs 5–7. For this simulation, $k_a[E] = 0.25 \text{ s}^{-1}$; $k_{\text{cat}} = k_d = 0.025 \text{ s}^{-1}$. The steady-state value for λ_{ES} is 0.901.

achieves its equilibrium value of $\theta_{ES}^{\text{eq}} = 0.909$, as determined from the Langmuir isotherm (eq 11).

The surface coverage of ES is not constant during the course of this reaction because the surface is rapidly being converted to the final product, S^* . However, the surface coverage of both the intermediate ES and the total number of unreacted sites are decreasing with time at the same rate. To show this, we also plot in Figure 2 the fraction of unreacted surface sites that are occupied by the enzyme, which we define as λ_{ES} :

$$\lambda_{ES} = \frac{\theta_{ES}}{\theta_{ES} + \theta_S} = \frac{\theta_{ES}}{1 - \theta_{S^*}} \quad (12)$$

Surprisingly, in Figure 2, λ_{ES} rises to a steady-state value of 0.728 that does not change as the surface is depleted. This steady-state value is below that of the equilibrium value of 0.909. If we make k_{cat} 10 times smaller, the kinetic simulation changes as shown in Figure 3. The relative surface coverage of ES rises to a value of 0.7 and then decreases at considerably slower rate than that shown in Figure 2. However, λ_{ES} rises close to the steady-state Langmuir isotherm equilibrium value and remains constant.

The dependence of the steady-state value of λ_{ES} on both k_{cat} and $k_a[E]$ can be determined analytically. The rate of change of λ_{ES} can be written as

$$\frac{d\lambda_{ES}}{dt} = \frac{1}{1 - \theta_{S^*}} \frac{d\theta_{ES}}{dt} + \frac{\theta_{ES}}{(1 - \theta_{S^*})^2} \frac{d\theta_{S^*}}{dt} \quad (13)$$

To find the steady-state value of λ_{ES} , eq 13 is set to zero and after solving for λ_{ES} yields

$$\lambda_{ES} = - \frac{d\theta_{ES}}{dt} \left[\left(\frac{d\theta_{S^*}}{dt} \right)^{-1} \right] \quad (14)$$

(25) Copeland, R. A. *Enzymes: A practical introduction to structure, mechanism and data analysis*; Wiley-VCH: New York, 2000; Vol. 2, pp 109–145.

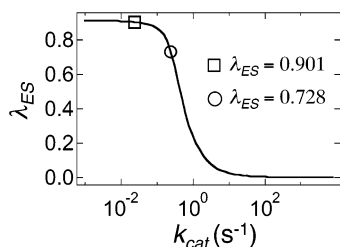


Figure 4. Variation in the steady-state value of λ_{ES} as a function of $\log k_{cat}$ with the values of $k_a[E] = 0.25 \text{ s}^{-1}$ and $k_d = 0.025 \text{ s}^{-1}$. (○) represents the value of λ_{ES} (0.728) when $k_{cat} = k_a[E] = 0.25 \text{ s}^{-1}$ and (□) shows the value of λ_{ES} (0.901) when $k_{cat} < k_a[E]$ with $k_{cat} = 0.025 \text{ s}^{-1}$.

Substitution of eqs 6 and 7 into eq 14 yields after rearrangement:

$$\lambda_{ES} = -\frac{k_a[E]}{k_{cat}\lambda_{ES}} + \frac{(k_a[E] + k_d + k_{cat})}{k_{cat}} \quad (15)$$

Equation 15 is a quadratic equation for λ_{ES} which can be solved with the quadratic formula using the appropriate root to yield the steady-state value of λ_{ES} observed in the kinetic simulations. Figure 4 plots the variation in λ_{ES} obtained using eq 15 as a function of k_{cat} with fixed values of $k_a[E] = 0.25 \text{ s}^{-1}$ and $k_d = 0.025 \text{ s}^{-1}$. The steady-state value of λ_{ES} depends on the relative values of k_{cat} , $k_a[E]$, and k_d . Note that, as k_{cat} decreases, λ_{ES} approaches the Langmuir equilibrium value of 0.909. When k_{cat} is equal to $k_a[E]$, a steady-state value of $\lambda_{ES} = 0.728$ is obtained, which is exactly the value observed in Figure 2. As k_{cat} becomes larger than $k_a[E]$, λ_{ES} approaches zero. If k_{cat} is much larger than $k_a[E]$, the velocity of the surface enzyme reaction will be solely limited by the enzyme adsorption kinetics. These equations demonstrate that, just as in the simple case when k_{cat} is small, there is a dynamic steady-state equilibrium set up for *ES*. However, it is the fractional surface coverage of *ES* relative to the number of unreacted sites (λ_{ES}) that remains constant, even as the total number of unreacted sites (θ_{ES}) goes to zero as the surface reaction is completed.

C. Diffusion Contributions to the Surface Enzymatic Reaction. In the kinetic analysis described above, we have not yet considered the possibility that enzyme diffusion to the gold surface may have an influence on the time-resolved SPR signal. Specifically, if diffusion is important, the bulk enzyme concentration $[E]$ in eq 6 should be replaced by the enzyme concentration at the surface. The effect of diffusion on Langmuir adsorption and desorption kinetics has been examined in detail in the SPR literature^{26–29} and in related electrochemical literature.^{8,30} For the case of a microfluidic flow cell such as the one used in our SPR kinetics measurements, a steady-state diffusion layer of thickness δ is created and eq 6 must be modified. In the absence of catalytic activity ($k_{cat} = 0$), diffusion contributions to the rate of enzyme adsorption can be included using the following differential equation:⁸

$$\frac{d\theta_{ES}}{dt} = \frac{k_a[E](1 - \theta_{ES}) - k_d\theta_{ES}}{1 + \beta(1 - \theta_{ES})} \quad (16)$$

where β is a dimensionless parameter:

$$\beta = \frac{k_a\Gamma_{tot}\delta}{D} = \frac{k_a\Gamma_{tot}}{k_m} \quad (17)$$

which compares the rate of adsorption to the rate of diffusion, where D is the diffusion constant for the enzyme and $k_m = D/\delta$ is the mass transfer coefficient. We can rederive this equation to include catalytic activity ($k_{cat} \neq 0$):

$$\frac{d\theta_{ES}}{dt} = \frac{k_a[E](1 - \theta_{ES} - \theta_{S^*}) - k_d\theta_{ES} - k_{cat}\theta_{ES}}{1 + \beta(1 - \theta_{ES} - \theta_{S^*})} \quad (18)$$

Equation 18 can be used as a direct replacement for eq 6.

Equation 16 has been derived previously by Saveant et al.⁸ for rotating disk electrodes and by Shuck and Minton²⁷ using a “two compartment model”. This model is used frequently in the SPR literature to include any diffusion contributions.²⁹ To experimentally confirm that there is a diffusion contribution, it is necessary to measure the flow-rate dependence of the SPR response.³¹ If there is a flow rate dependence, eq 16 can be integrated and the SPR adsorption curves can be analyzed to determine the Langmuir adsorption coefficient. If there is no flow-rate dependence of the SPR response, the effects of diffusion can be ignored and the adsorption coefficient can be ascertained from the standard equations for Langmuir adsorption kinetics.²

For all of the Exo III surface enzyme kinetics examined in this paper at various enzyme concentrations and reaction temperatures, no significant changes in the SPR response were observed for flow rates from 30 to 1000 $\mu\text{L}/\text{min}$. This indicates that mass transport has a negligible role in determining the overall reaction rate under our experimental conditions.

A second method for examining possible diffusion contributions is to use eq 17 to estimate the parameter β . With a molecular weight of 28 000 Da, the Exo III diffusion coefficient can be estimated³² to be $10^{-6} \text{ cm}^2\cdot\text{s}^{-1}$. Assuming a diffusion layer thickness of $5 \mu\text{m}$ ²⁶ and a double-stranded DNA (dsDNA) surface coverage of $5 \times 10^{-13} \text{ moles}\cdot\text{cm}^{-2}$, we find that $\beta = 10^{-7}k_a$. Subsequent data analysis indicates a k_a value for Exo III binding to be close to $10^5 \text{ M}^{-1}\cdot\text{s}^{-1}$, suggesting a value of 0.01 for β . This small value for β agrees with our experimental finding that the SPR response did not change with flow rate.

A second diffusion contribution that is neglected in this kinetic analysis is any lateral diffusion of the enzyme along the surface prior to complexation. In some enzyme systems, adsorption to the surface can occur without complexation to the substrate. This was the case for the system studied by Gast et al.¹² However, for Exo III, adsorption was never observed on control array elements where the dsDNA substrate was absent. We therefore do not include a surface population of adsorbed but uncomplexed enzymes in our kinetic equations nor any contributions due to lateral diffusion of adsorbed but uncomplexed enzymes on the surface.

III. Experimental Section

Materials. 11-Mercaptoundecylamine (MUAM; Dojindo), sulfosuccinimidyl 4-(*N*-maleimidomethyl)-cyclohexane-1-carboxylate (SSMCC; Pierce), 9-fluorenylmethoxycarbonyl-*N*-hydroxy-

(26) Karlsson, R.; Roos, H.; Fagerstam, L.; Persson, B. *Methods* **1994**, *6*, 99–110.

(27) Schuck, P.; Minton, A. P. *Anal. Biochem.* **1996**, *240*, 262–272.

(28) Myszkka, D. G. *Curr. Opin. Biotechnol.* **1997**, *8*, 50–57.

(29) Myszkka, D. G.; He, X.; Dembo, M.; Morton, T. A.; Goldstein, B. *Biophys. J.* **1998**, *75*, 583–594.

(30) Bhugun, I.; Anson, F. C. *J. Electroanal. Chem.* **1997**, *439*, 1–6.

(31) Myszkka, D. G.; Morton, T. A.; Doyle, M. L.; Chaiken, I. M. *Biophys. Chem.* **1997**, *64*, 127–137.

(32) Christensen, L. L. H. *Anal. Biochem.* **1997**, *249*, 153–164.

succinimide (Fmoc-NHS; Novabiochem), *N*-hydroxysuccinimidyl ester of methoxypoly(ethylene glycol) propionic acid (PEG-NHS; Nektar; MW 2000), and Exonuclease III (Exo III; Promega; 1 U/mL = 0.17 nM) were all used as received. Tris buffer (50 mM Tris-HCl, 10 mM MgCl₂, pH 7.4) was used for all Exo III experiments. All of either 5' or 3' thiol-modified DNA oligonucleotides were purchased from IDT (Integrated DNA Technologies) and were purified and deprotected using binary reverse-phase HPLC. The complementary DNA (HPLC purified) was obtained commercially from IDT (Integrated DNA Technologies). The DNA oligonucleotides used in these experiments are as follows: D₁ = 3' S-S(CH₂)₃A₂₀, D₂ = 5' S-S(CH₂)₆T₂₀ and C₁ = 5'(T)₂₀. All rinsing steps were performed with absolute ethanol and Millipore filtered water.

DNA Array Fabrication. A multistep chemical modification process was used to fabricate DNA microarrays for SPR imaging experiments and can be found elsewhere.^{23,33} Briefly, thin gold films (45 nm) with an underlayer of chromium (1 nm) were deposited onto SF-10 glass (Schott Glass) using a Denton DV-502A metal evaporator. The gold substrate was reacted to form a self-assembled monolayer (SAM) of an amine-terminated alkanethiol MUAM. The amine-terminated SAM was then reacted with the temporary hydrophobic protecting group Fmoc-NHS. By exposing the surface to UV radiation through a quartz mask containing 500 μm × 500 μm features, patterns of bare gold spots surrounded by the hydrophobic background were created. The bare gold spots were then modified with MUAM and spotted with the heterobifunctional cross-linker SSMCC to form a thiol-reactive maleimide-terminated surface. Thiol-modified sequences of DNA were then spotted into these hydrophilic array elements using a pneumatic picopump. To avoid the nonspecific adsorption of enzyme and cleaved product, the Fmoc background was replaced with poly(ethylene glycol) (PEG) after deprotection. The surface coverage of the single-stranded DNA (ssDNA) monolayer was estimated to be approximately 1 × 10¹² molecules/cm².

Kinetic Flow Cell Design. A PDMS microfluidics system previously developed² was used to continuously deliver small sample volumes onto an array surface for kinetics measurements. Briefly, a serpentine PDMS microchannel (670 μm width, 9.5 cm length, 200 μm depth, total volume ≈ 10 μL) was pretreated with oxygen plasma for 10 s and placed in direct contact with the array surface. Oxygen plasma treatment enhances the hydrophilicity of the PDMS channels thus facilitating the introduction of aqueous samples, as well as reducing biomolecular adsorption onto the walls of the channels. A constant temperature sample/prism holder was used in conjunction with the microfluidics in order to reduce any fluctuations in SPR signal over time due to temperature variations. The details of the constant temperature cell can be found elsewhere.^{1,2} Buffer and/or sample solutions were introduced to the array using a syringe pump at a constant flow rate of 30 μL/min.

Real-Time SPR Imaging Measurements. An SPR imaging apparatus (GWC Technologies) was used for the real-time monitoring of the hydrolysis of DNA microarrays by Exo III. Briefly, a collimated p-polarized light at a fixed angle reflected from the sample/gold/prism assembly is sent through a narrow band-pass filter and then detected with a CCD camera. The data are collected using the software package V++ (Digital Optics, NZ). Custom macros were written using this software so that data could be collected with simultaneous processing of several specific user designated regions of interest (ROIs) on the array surface.² All kinetics experiments presented in this paper were obtained by collecting one data point for each ROI approximately every 1 s that was the average of five camera frames. The difference in percent reflectivity for each probe area was normalized with respect to the average change in percent reflectivity measured for the PEG background and negative control ROIs. This helps account for changes in the SPR signal due to miscellaneous factors such as slight temperature variations and bulk refractive index changes. Kinetic data from multiple identical array elements were averaged to obtain the final SPR response curves. Microsoft Excel and Igor Pro were used for all data processing and kinetic model fitting in these experiments.

(33) Brockman, J. M.; Frutos, A. G.; Corn, R. M. *J. Am. Chem. Soc.* **1999**, *121*, 8044–8051.

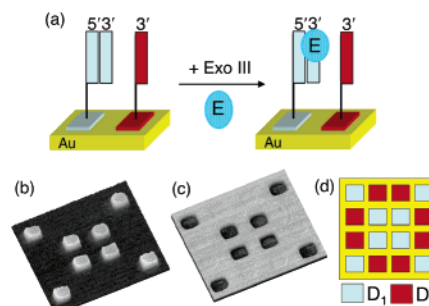


Figure 5. (a) Schematic representation of 3' → 5' exodeoxyribonuclease activity of Exo III specific for double-stranded DNA microarrays. (b) An SPR difference image showing the sequence specific hybridization adsorption of 500 nM complementary DNA (C₁) onto D₁ array elements. (c) An SPR difference image obtained after an 80 nM solution of Exo III is introduced to the DNA microarray shown in (b) for 40 min. (d) The pattern used to create a two-component DNA microarray using thiol-modified DNA sequences (D₁ and D₂). Array elements are 500 μm × 500 μm squares. Probe D₁ was designed to bind to the target DNA C₁, and probe sequence D₂ was chosen as a negative control.

IV. Results and Discussion

A. Exonuclease III Specificity. Exo III is widely used in various DNA manipulative procedures such as DNA repair, site-directed mutagenesis, and the production of strand-specific probes.^{34–38} In this section, we focus on investigating the 3' → 5' exodeoxyribonuclease activity of Exo III, which involves specific binding to double-stranded DNA followed by selective hydrolysis of one strand from the DNA duplex. Figure 5a shows a schematic of the strand-specific hydrolysis reaction of Exo III on a DNA microarray. A two-component array was fabricated. (i) DNA probe D₁, which is surface-tethered via thiol modification of the 3' end and (ii) the second DNA sequence D₂ acts as a control probe and is 5' thiol modified. Exo III will specifically bind to the dsDNA, but not to the single-stranded DNA, and start converting dsDNA molecules to ssDNA. The Exo III enzyme reaction can therefore be used to identify hybridization adsorption onto ssDNA microarrays. The Exo III enzyme will not digest the other DNA strand (DNA probe D₁) in the duplex because the 3' end of this DNA strand is attached to the surface. An advantage of this approach is that the DNA array can be used repeatedly by simply denaturing any remaining dsDNA with urea and rinsing with buffer.

In a first step, a two component ssDNA array (D₁ and D₂) is exposed to the target complementary DNA sequence (C₁) resulting in duplex formation of D₁ array elements. Figure 5b shows an SPR difference image obtained after a 500 nM solution of C₁ was introduced to the DNA array at room temperature (25 °C). An increase in the Δ%R was observed only on D₁ elements, indicating sequence-specific hybridization adsorption and the formation of dsDNA on the surface. Upon Exo III injection onto the array, the enzyme selectively binds to the 3' end of C₁ in the D₁–C₁ duplex and sequentially releases 5'-mononucleotides into the bulk solution. Figure 5c shows a difference image after exposure to an 80 nM solution of Exo III for 40 min. It can

(34) Weiss, B. In *The enzymes*, 3rd ed.; Boyer, P. B., Ed.; Academic Press, Inc.: New York, 1981; Vol. 14, pp 203–231.

(35) Okano, K.; Kambara, H. *Anal. Biochem.* **1995**, *228*, 101–108.

(36) Mol, C. D.; Kuo, C.; Thayer, M. M.; Cunningham, R. P.; Tainer, J. A. *Nature* **1995**, *374*, 381–386.

(37) Brakmann, S.; Lobermann, S. *Angew. Chem., Int. Ed.* **2002**, *41*, 3215–3217.

(38) Greenberg, M. M.; Weledji, Y. N.; Kim, J.; Bales, B. C. *Biochemistry* **2004**, *43*, 8178–8183.

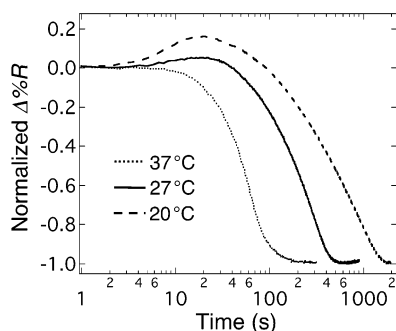


Figure 6. Plot showing the kinetic data obtained at various reaction temperatures (20, 27, and 37 °C) for the hydrolysis of dsDNA microarrays at an Exo III concentration of 80 nM. The semilogarithmic time plot is used to highlight differences during the initial stages of the enzymatic reaction.

be clearly seen that Exo III has hydrolyzed C_1 strands from the D_1 - C_1 duplex but has not affected the single-stranded D_2 array elements. Moreover, the Exo III did not affect the D_1 ssDNA, so this hybridization/hydrolysis cycle could be repeated up to 20 times without any significant degradation in the SPR imaging signal. Additionally, in both reaction steps, nonspecific binding of C_1 or enzyme to either the D_2 control spots or the PEG background was not observed. The complete recovery of the $\Delta\%R$ signal to initial values at higher enzyme concentrations also confirms that after hydrolysis the enzyme does not remain on the array surface.

B. Temperature Dependence. Temperature is known to play a significant role in determining the level of exonuclease activity of Exo III. For example, between 22 and 46 °C, Exo III activity in solution increases proportionally with temperature, doubling approximately every 6 °C.³⁹ Figure 6 shows real-time SPR imaging data obtained at various reaction temperatures for a bulk enzyme concentration of 80 nM. In each case, the SPR signal was normalized with respect to the magnitude of the $\Delta\%R$ associated with the hybridization reaction step. The time axis is plotted on a logarithmic scale to highlight prominent differences during the early reaction stages. The time scale required for complete cleavage of the dsDNA microarray varied markedly, with values of 150, 490, and 1700 s measured at 37, 27, and 20 °C, respectively. At an enzyme concentration of 80 nM, the rate of complete removal of a 20-mer DNA strand can be estimated to be 8, 2.5, and 0.7 nucleotides/min at 37, 27, and 20 °C, respectively. This is much lower than the range of 100–600 nucleotides/min at 25–41 °C measured in solution for a saturating enzyme concentration of 120 U Exo III/ μ g DNA.³⁹ The large variation between surface and bulk cleavage rates can be attributed to a reduction in steric freedom at the surface. As in the solution measurements, the large variation in surface enzyme reaction times reflects the strong dependence of Exo III surface activity on temperature.

It is important to note that the SPR signal is the sum of two components—an increase due to enzyme adsorption and a loss due to substrate cleavage. The measured SPR signal increases initially in response to the ES complex formation but eventually decreases significantly due to the loss of the C_1 complementary DNA sequence. At 37 °C, no net increase in the SPR signal was observed during the early reaction stages. This suggests that the rate of loss of surface bound species remains greater than the rate of ES formation throughout the whole reaction period.

At lower temperatures (27 and 20 °C), a pronounced initial rise in signal is observed, suggesting that the rate of enzyme adsorption must exceed the rate of duplex cleavage over the same initial period. It is noted that a significant increase in the activation energy associated with solution exonuclease activity has been reported³⁹ to occur at temperatures below 25 °C. Additionally, higher processivity, which alludes to the average number of individual nucleotides sequentially cleaved in a single enzymatic action, also plays a much more prominent role at lower temperatures.⁴⁰ Therefore, it is reasonable to expect that, due to the lower catalytic activity, the average residence time of an enzyme molecule on the surface in the form of the ES complex will be considerably longer at lower temperatures, thus contributing to the observed initial increase in SPR imaging signal.

C. Analysis of Exo III Reaction at 20 °C. To achieve further insight into the relative contributions of the enzymatic adsorption and cleavage steps toward the overall reaction rate, kinetics data were acquired using several enzyme bulk concentrations at a fixed temperature of 20 °C. The data were then analyzed by applying the model introduced previously in Section II. Here, the changes in the relative surface coverages of the ES complex (θ_{ES}) and the cleaved ssDNA product (θ_{S^*}) over the reaction course are controlled using three different parameters, k_a , k_d , and k_{cat} . The time-dependent SPR signal ($\Delta\%R$) is normalized with respect to the magnitude of $\Delta\%R$ associated with the hybridization reaction step. The normalized signal responds to both enzyme adsorption and surface loss of the C_1 DNA complement and can be represented by

$$\Delta\%R(t) \propto A\theta_{ES} - \theta_{S^*} \quad (19)$$

where A is a weighting factor. This is necessary to consider since Exo III has a molecular weight (28 000 Da) considerably larger than the C_1 DNA complement (6447 Da). This suggests a weighting factor of around 4; however, it must be noted that the surface density of the DNA duplex monolayer is much higher than the surface enzyme coverage. Additionally, differences in the binding affinity of the ES complex and the D_1 - C_1 duplex may have an impact on their relative SPR signal contributions. When analyzing our data, we applied weighting factor values ranging from 1 to 4 and found the best model fit using a value of $A = 1$. Additional fluorescence measurements^{12,16} would allow us to ascertain the value of the weighting factor.

Figure 7 compares theoretical analysis and experimental measurements when a 320 nM Exo III solution is continually passed over a prepared dsDNA microarray at 20 °C. A global curve fitting approach was adopted to simultaneously analyze a series of experimental curves acquired at several different enzyme concentrations and to determine the best values for the three model parameters (k_a , k_d , and k_{cat}). By applying eqs 5–7 and 19, values of $k_a = 2.2 \times 10^5 \text{ M}^{-1}\text{s}^{-1}$, $k_d = 0.056 \text{ s}^{-1}$, and $k_{cat} = 0.009 \text{ s}^{-1}$ were obtained. Using these values, the Langmuir adsorption coefficient (K_{Ads}) is $3.9 \times 10^6 \text{ M}^{-1}$ and the surface Michaelis–Menten constant (K'_M) in eq 9 is 300 nM. The simulated SPR signal using these values for an enzyme concentration of 320 nM is shown in Figure 7b. It is clear that there is a very good agreement between the measured and simulated SPR signals.

Simulated plots of the different relative surface coverages are also presented in Figure 7. At an enzyme

(39) Hoheisel, J. D. *Anal. Biochem.* **1993**, *209*, 238–246.

(40) Kow, Y. W. *Biochemistry* **1989**, *28*, 3280–3287.

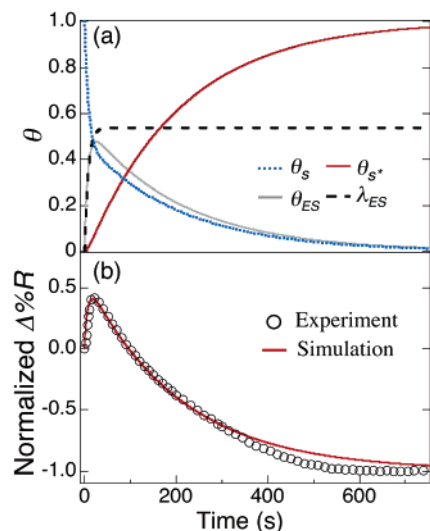


Figure 7. (a) Theoretical analysis of the enzyme reaction using eqs 5–7 and $k_a = 2.2 \times 10^5 \text{ M}^{-1}\cdot\text{s}^{-1}$, $[E] = 320 \text{ nM}$, $k_d = 0.056 \text{ s}^{-1}$, and $k_{\text{cat}} = 0.009 \text{ s}^{-1}$. The steady-state value for λ_{ES} is 0.54. (b) The real-time SPR response (○) obtained for Exo III (320 nM) cleavage reaction onto D₁ dsDNA array elements at 20 °C. The dsDNA array was created by sequence-specific hybridization of C₁ complementary sequences to two-component ssDNA arrays composed of D₁ and D₂. The solid line represents the simulated kinetic curve fitted using eqs 5–7 and 19 with the same k_a , k_d , and k_{cat} values reported above.

concentration of 320 nM, $k_a[E] = 0.07 \text{ s}^{-1}$, which is eight times greater than k_{cat} . The relative surface coverage of *ES* (θ_{ES}) quickly rises compared to the rate of C₁ loss (θ_{S^*}) before reaching a maximum of 0.46 and slowly decreasing. λ_{ES} rises to a steady-state value of 0.54, which is about equal to the calculated steady-state Langmuir isotherm equilibrium value (θ_{ES}^{eq} in eq 11) of 0.56. The closeness of these values indicates a significant but varying enzyme coverage in the form of the *ES* complex, as expected from Figure 4. When k_{cat} is increased with respect to $k_a[E]$ (by either increasing the reaction temperature to 37 °C or decreasing $[E]$), λ_{ES} will reach a steady-state value lower than 0.54, reflecting a reduced intermediary *ES* complex surface coverage.

The experimental and corresponding theoretical curves obtained for enzyme concentrations varying from 50 to 320 nM are summarized in Figure 8. All the simulated curves use the same values of k_a , k_d , and k_{cat} quoted above. The experimental data shown in this figure were obtained using the same microarray by recovering the original ssDNA surface through the use of urea to denature any remaining duplex and rinsing with buffer between concentration runs. The measured SPR kinetic responses were successfully analyzed with the theoretical model over the entire range of enzyme concentrations studied. The ability of the expected model to fit the data can be further tested by examining $T_{50\%}$, the time at each curve associated with 50% depletion of single-stranded complementary (C₁) from the duplex monolayer, as a function of enzyme concentration. Figure 9 plots experimental data (○) and the values calculated from the theory (▲). A series of repeated measurements at 20 °C using the same batch of enzyme showed an excellent reproducibility of $T_{50\%} = \pm 5\%$ over a number of chips prepared in an identical manner. The dependence of $T_{50\%}$ on $[E]$ varies more rapidly at lower enzyme concentrations (below 100 nM). The theory predicts that at very high enzyme concentrations ($\geq 5 \mu\text{M}$) $T_{50\%}$ approaches a value of 156 s. This value depends on k_a , k_d , and k_{cat} . The excellent fit of theory and experiment in this figure clearly shows that the model constructed

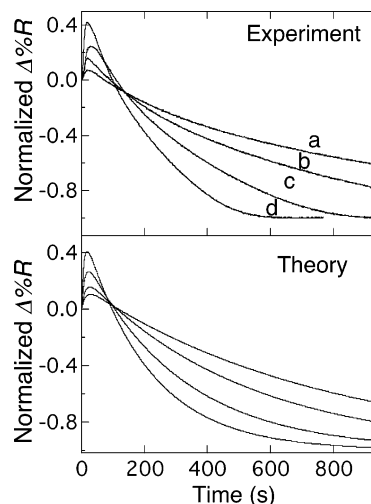


Figure 8. Top: Compiled experimental kinetic data obtained at various concentrations of Exo III for the hydrolysis of D₁–C₁ duplexes at a temperature of 20 °C. The enzyme concentrations (a, b, c, and d) are 50, 80, 160, and 320 nM, respectively. Bottom: Simulated kinetic curves of the enzyme reaction fitted using eqs 5–7 and 19 at the same enzyme concentrations as in (a, b, c, and d) with the parameters $k_a = 2.2 \times 10^5 \text{ M}^{-1}\cdot\text{s}^{-1}$, $k_d = 0.056 \text{ s}^{-1}$, and $k_{\text{cat}} = 0.009 \text{ s}^{-1}$.

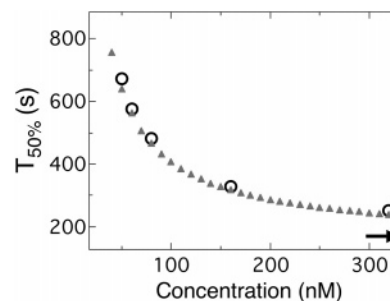


Figure 9. Plot of reaction times at 50% of observed SPR signal decrease ($T_{50\%}$) versus Exo III enzyme concentrations. (○) is the experimental data and (▲) represents the calculated values from the simulated data in Figure 8. The arrow represents the limiting $T_{50\%}$ value predicted by theory at very high enzyme concentrations ($\geq 5 \mu\text{M}$).

quantitatively describes the surface enzyme reaction and emphasizes the importance of the coupling of enzyme adsorption and surface reaction kinetics on the observed reaction rate.

V. Conclusions

In this paper, we introduced a kinetic model that can be used to analyze real-time kinetic measurements of surface enzymatic activity using the technique of SPR imaging. By combining the concepts associated with Langmuir adsorption kinetics and Michaelis–Menten analysis, it is possible to characterize the enzymatic reaction in terms of three simple parameters (k_a , k_d , and k_{cat}). In classical Michaelis–Menten studies where the substrate concentration is typically far in excess of the enzyme concentration, the concentration of the intermediary *ES* complex (θ_{ES}) can be assumed to be constant. However, this assumption cannot be applied to surface reactions where the substrate surface concentration is finite and eventually goes to zero as the reaction is completed. Instead, the fractional *ES* surface coverage of unreacted sites (λ_{ES}) reaches a constant value during the course of the surface enzyme reaction.

The importance of the relative magnitudes of the rate of adsorption ($k_a[E]$) and catalysis (k_{cat}) on the overall reaction rate was demonstrated by studying the 3' → 5' cleavage activity of Exonuclease III on dsDNA microarrays. The experiments at 20 °C show that the value of λ_{ES} is comparable to the Langmuir equilibrium value (θ_{ES}^{eq}). In contrast, λ_{ES} becomes smaller at higher temperatures due to increases in k_{cat} . Further analysis of the Exo III reaction at 37 °C will be discussed in a subsequent paper.

Finally, the surface exonuclease reaction analyzed in this paper represents only one of many possible enzymatic reactions that can be incorporated into the multiplexed surface biosensor array format. Enzymes such as proteases, kinases, and ligases can all be used to manipulate surface populations of biomolecules in order to achieve higher sensitivity or specificity in bioassays. The analysis of the Exo III surface reactions described in this paper clearly shows that a coupled approach combining both enzyme adsorption kinetics and enzymatic surface ca-

talyses rates is required to quantitatively understand surface enzymatic activity. Future work will focus on the application of similar kinetic models to other surface enzyme reactions. The very simple model proposed here applies only to systems where the enzyme binds specifically to a surface target in a 1:1 interaction in the absence of mass transport limitations. More complex models involving, for example, multiple binding sites, such as a transcription factor protein or lateral surface diffusion between binding partners in membranes, will be required for the analysis of more complex biochemical surface processes.

Acknowledgment. This research is funded by the National Institute of Health (2RO1 GM059622-04), the National Science Foundation (CHE-0133151), and a start-up grant from University of California, Irvine.

LA046822H